[15] I. B. Rother, E. Freisinger, A. Erxleben, B. Lippert, *Inorg. Chim. Acta* **2000**, *300*, 339.
[16] J. P. Garcia-Teran, O. Castillo, A. Luque, U. Garcia-Couceiro, P. Roman, F. Lloret, *Inorg. Chem.* **2004**, *43*, 5761.
[17] J. P. Garcia-Teran, O. Castillo, A. Luque, U. Garcia-Couceiro, P. Roman, L. Lezama, *Inorg. Chem.* **2004**, *43*, 4549.
[18] a) M. A. Shipman, C. Price, A. E. Gibson, M. R. J. Elsegood, W. Clegg, A. Houlton, *Chem. Eur. J.* **2000**, *6*, 4371. b) M. A. Shipman, C. Price, M. R. J. Elsegood, W. Clegg, A. Houlton, *Angew. Chem. Int. Ed.* **2000**, *39*, 2360.
[19] P. J. de Pablo, F. Moreno-Herrero, J. Colchero, J. G. Herrero, P. Herrero, A. M. Baro, P. Ordejon, J. M. Soler, E. Artacho, *Phys. Rev. Lett.* **2000**, *85*, 4992.
[20] C. Gomez-Navarro, F. Moreno-Herrero, P. J. de Pablo, J. Colchero, J. Gomez-Herrero, A. M. Baro, *Proc. Natl. Acad. Sci. USA* **2002**, *99*, 8484.
[21] A. J. Storm, J. van Noort, S. de Vries, C. Dekker, *Appl. Phys. Lett.* **2001**, *79*, 3881.
[22] a) D. Porath, G. Cuniberti, R. Di Felice, *Top. Curr. Chem.* **2004**, *237*, 183. b) R. G. Endres, D. L. Cox, R. R. P. Singh, *Rev. Mod. Phys.* **2004**, *76*, 195.
[23] A. Houlton, *Adv. Inorg. Chem.* **2002**, *53*, 87.
[24] T. Carell, C. Behrens, J. Gierlich, *Org. Biomol. Chem.* **2003**, *1*, 2221.
[25] P. Aich, S. L. Labiuk, L. W. Tari, L. J. T. Delbaere, W. J. Roesler, K. J. Falk, R. P. Steer, J. S. Lee, *J. Mol. Biol.* **1999**, *294*, 477.
[26] J. S. Lee, L. J. P. Latimer, R. S. Reid, *Biochem. Cell Biol.* **1993**, *71*, 162.
[27] A. Rakitin, P. Aich, C. Papadopoulos, Y. Kobzar, A. S. Vedeneev, J. S. Lee, J. M. Xu, *Phys. Rev. Lett.* **2001**, *86*, 3670.
[28] A. Calzolari, R. Di Felice, E. Molinari, A. Garbesi, *Appl. Phys. Lett.* **2002**, *80*, 3331.
[29] U. García-Couceiro, D. Olea, O. Castillo, A. Luque, P. Romàn, P. J. de Pablo, J. Gómez-Herroro, F. Zamora, unpublished.
[30] www.nanotec.es
[31] P. J. de Pablo, M. T. Martinez, J. Colchero, J. Gomez-Herrero, W. K. Maser, A. M. Benito, E. Munoz, A. M. Baro, *Adv. Mater.* **2000**, *12*, 573.
[32] E. Dubler, E. Gyr, *Inorg. Chem.* **1988**, *27*, 1466.
[33] P. J. de Pablo, C. Gomez-Navarro, A. Gil, J. Colchero, M. T. Martinez, A. M. Benito, W. K. Maser, J. Gomez-Herrero, A. M. Baro, *Appl. Phys. Lett.* **2001**, *79*, 2979.
[34] J. M. Soler, E. Artacho, J. D. Gale, A. Garcia, J. Junquera, P. Ordejon, D. Sanchez-Portal, *J. Phys. Condens. Matter* **2002**, *14*, 2745.
[35] J. P. Perdew, K. Burke, M. Ernzerhof, *Phys. Rev. Lett.* **1996**, *77*, 3865.
[36] N. Troullier, J. L. Martins, *Phys. Rev. B* **1991**, *43*, 1993.
[37] S. S. Alexandre, E. Artacho, J. M. Soler, H. Chacham, *Phys. Rev. Lett.* **2003**, *91*, 108 105.

Controlled Nanoscale Morphology of Hematite (0001) Surfaces Grown by Chemical Vapor Transport**

By *Mark E. Greene*, *Ann N. Chiaramonti*, *Steven T. Christensen*, *Lixin Cao*, *Michael J. Bedzyk*, and *Mark C. Hersam**

Hematite (α-Fe_2O_3) has demonstrated value as an important material component in several advanced technological applications, including heterogeneous catalysis,[1] photoelectrochemistry,[2,3] dyes and stains,[4] magnetic data storage,[5] and room-temperature magnetic semiconductors.[6,7] The structure and properties of hematite also have critical implications in the fabrication and corrosion of steels, geochemistry, and planetary science.[8] Additionally, novel hematite nanostructures have been synthesized, including nanoparticles[9] and porous nanorods,[10] which exhibit interesting magnetic properties and may find use in emerging technologies.

The origin of the diverse set of applications of hematite can be traced to its electronic structure. Pure hematite is an antiferromagnetic charge-transfer semiconductor with a bandgap of approximately 2 eV and a canted structure that leads to net magnetization.[6,11,12] Furthermore, recent calculations suggest that hematite doped with Ti atoms on alternate Fe sublattice layers is a ferrimagnetic semiconductor with spin-dependent transport properties and a magnetic transition temperature of around 700 °C.[7] Bulk hematite adopts the corundum crystal structure[13] (space group $R\bar{3}c$), as shown in Figure 1a. The hematite crystal in the figure is in the basal-plane orientation with the (0001) surface terminated by an Fe layer (Fe–O_3–Fe–⋯ termination).

For several potential applications, such as heterogeneous catalysis, the hematite surface plays a crucial role. Therefore, a detailed knowledge of the hematite surface structure and properties is needed to understand and further engineer this material for applications. For example, in the presence of UV radiation, hematite promotes the photocatalytic degradation of SO_2[2] and aminophenols,[3] two atmospheric pollutants, at reactive surface sites created through the excitation of elec-

[*] Prof. M. C. Hersam, M. E. Greene, A. N. Chiaramonti, S. T. Christensen, Dr. L. X. Cao, Prof. M. J. Bedzyk
Department of Materials Science and Engineering, and the Institute for Environmental Catalysis, Northwestern University
2220 Campus Drive, Evanston, IL 60208-3108 (USA)
E-mail: m-hersam@northwestern.edu

[**] We thank Prof. Mikio Takano of the Institute for Chemical Research at Kyoto University for supplying the CVT-grown hematite samples. In addition, we acknowledge informative discussions with Prof. Kenneth Poeppelmeier, Prof. Peter Stair, Prof. Laurence Marks, and Prof. Mark Asta at Northwestern University. This work was supported by the Department of Energy Institute for Environmental Catalysis, under Grant Number DE-FG02-03ER15457, and used Northwestern University MRSEC central facilities (NSF DMR-0076097).

 DOI: 10.1002/adma.200401459

ADVANCED MATERIALS

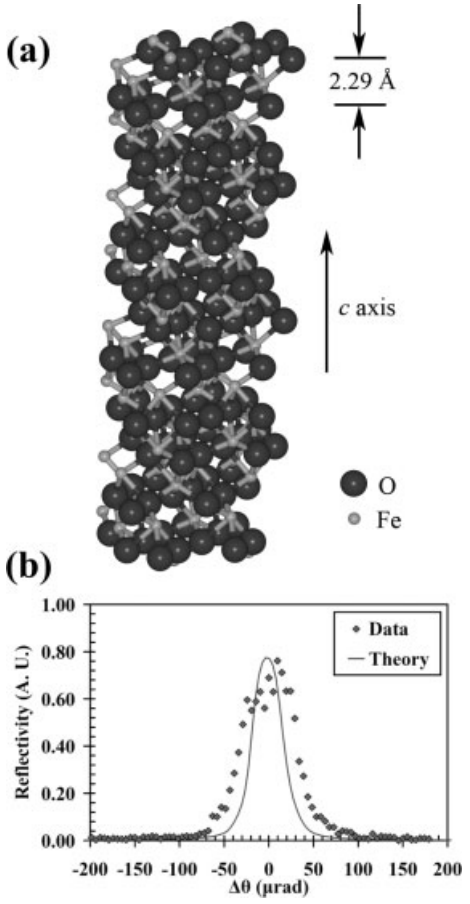

Figure 1. a) The hematite (α-Fe_2O_3) crystal structure with an Fe–O_3–Fe–⋯ termination. The crystal is tilted slightly to view the (0001) basal plane at the top more clearly. The distance separating adjacent O planes is indicated. b) Experimental and ideal theoretical (0006) rocking curves for chemical vapor transport (CVT)-grown hematite (0001).

tron–hole pairs. Since the chemical activity of the surface is related to the electronic structure and crystal reconstruction of the termination layers, as well as to the distribution of defects, atomic steps, impurities, and other features, optimization of these chemical processes is linked to controlling the hematite surface morphology. For these reasons, synthetic hematite may be more desirable than mineral hematite for many applications as the purity and doping can be tightly controlled by the precursor gases and growth conditions used for the crystal synthesis.

Despite avid interest in the development and use of hematite as a technological material, minimal data concerning the nanoscale morphological evolution of synthetic hematite surfaces at elevated temperatures have been presented in the literature. In perhaps the most extensive study to date, Shaikhutdinov and Weiss used low-energy electron diffraction and scanning tunneling microscopy (STM) to show the variation in surface structures that result when thin-film hematite is grown on Pt(111) over a range of O_2 partial pressures spanning six orders of magnitude, from 1 mbar down to 10^{-6} mbar (1 bar = 100 kPa) at temperatures in excess of 800 °C.[14] They observed that hexagonal corrugations, attributed to the Fe sublattice, increased in fractional surface coverage as the O_2 partial pressure was iteratively reduced during a sequence of surface preparations.

In this communication, we characterize the nanoscale morphology of the hematite (0001) surface using atomic force microscopy (AFM). AFM is well-suited for the study of oxide surfaces as these surfaces are generally not conductive enough to perform STM on them, unless prepared under special conditions. Following appropriate annealing conditions, we observe atomically flat domains on hematite (0001) that extend for tens of micrometers and are bounded by highly stepped regions. The atomically flat domains possess subnanometer-deep circular depressions that are qualitatively similar to the surface morphology of graphite[15–17] and $SrTiO_3$.[18] At room temperature, the observed surface morphology of hematite (0001) remains invariant following exposure to ambient conditions for time periods on the order of several months.

The hematite crystals were grown via a CVT technique, by using HCl gas as the transport agent according to the following reaction:[19,20]

$$Fe_2O_3(s) + 6\,HCl(g) \rightleftharpoons 2\,FeCl_3(g) + 3\,H_2O(g) \quad (1)$$

The growing hematite crystal was held in one zone at ~850 °C, while the source material was kept in a different zone at ~1000 °C. The crystals resulting from this treatment are termed "as-grown" in the remainder of this paper. Back-reflection Laue measurements confirmed that the as-grown CVT hematite crystals possess a (0001) orientation. In addition, X-ray rocking curves were gathered to assess crystal quality, as shown in Figure 1b. The dynamical diffraction theory simulated curve that is overlaid on the data in Figure 1b is a convolution of the ideal Si(111) monochromator reflectivity curve with the ideal hematite (0006). The fact that the experimental reflectivity curve is almost as narrow as the ideal theoretical curve characterizes the nearly perfect crystal quality of the CVT-grown hematite (0001) samples over the 4 mm^2 footprint of the incident beam.

The as-grown hematite (0001) crystals were subsequently annealed at 900 °C in air under atmospheric pressure, in pure oxygen, or in pure argon for 2 h using a tube furnace. The resulting surfaces following annealing in air or pure oxygen were the same, thus suggesting that oxygen (as opposed to another constituent of air) is critical to the evolution of the observed surface morphology. Figure 2 shows the intermittent contact mode AFM topography of the CVT hematite (0001) surface before and after annealing in an oxygen-rich environment. The as-grown surface in Figure 2a is relatively featureless with a root mean square roughness of 0.4 Å. After annealing in an oxygen-rich environment, the surface has undergone a transition to an atomically flat morphology with circular depressions, as seen in Figure 2b. It should be noted that the surface morphology following annealing in pure argon appeared the same as the as-grown surface, thus confirming the critical role of oxygen in the evolution of atomically flat circular domains on the CVT hematite (0001) surface.

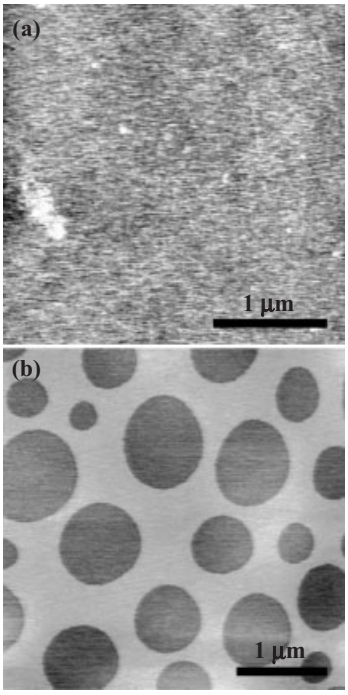

Figure 2. AFM images of CVT-grown hematite (0001) surfaces a) before and b) after annealing at 900 °C for 2 h in air, under atmospheric pressure. Image sizes are a) 3 μm × 3 μm and b) 3.77 μm × 3.77 μm. The root mean square roughness is 0.4 Å in (a), whereas the atomic step height is 2.2 ± 0.2 Å in (b).

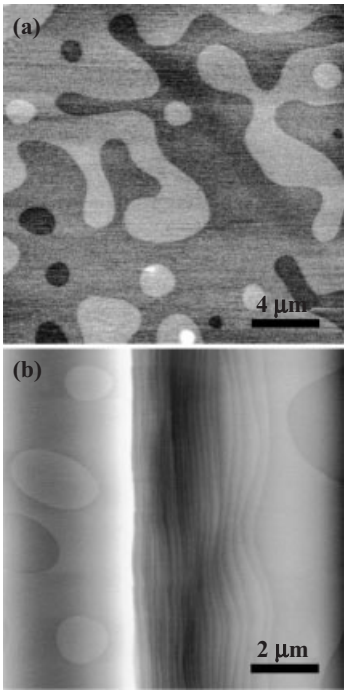

Figure 3. AFM images of CVT-grown hematite (0001) surfaces after annealing at 900 °C for 2 h in air, under atmospheric pressure. a) 20 μm × 20 μm image of an atomically flat domain where the circular features have apparently coalesced. b) 10 μm × 10 μm image of a highly stepped region that borders two atomically flat domains. In this case, the image flattening was chosen to accentuate the bunched steps, which leads to an artificial contrast variation along the atomically flat domains. The atomic step height in both images is 2.2 ± 0.2 Å.

The formation of an atomically flat surface morphology with circular features was observed on multiple CVT hematite (0001) samples. For example, Figure 3a illustrates a second CVT hematite (0001) surface following annealing in an oxygen-rich environment. In this case, the circular features have apparently coalesced to form a more complicated morphology. The atomically flat domains possess a broad spatial extent over distances of the order of tens of micrometers. Repeated AFM imaging has shown that this morphology is found on at least 90 % of the sample surface. At the boundary between atomically flat domains, step-bunching is observed, as shown in Figure 3b. The subtle differences between the surfaces in Figure 2b and Figure 3a may result from minor differences in the initial CVT-grown hematite (0001) samples (e.g., differences in miscut angle or impurity content). It should be noted that energy dispersive X-ray analysis did not indicate the presence of impurity segregation at the terraces, circular depressions, or step edges. Furthermore, images of the same surface following several months of storage in air at room temperature did not show any detectable change in the observed surface morphology.

The surface normal axis (z) of the AFM was calibrated using the known atomic step height of hydrogen-passivated Si(111). Following this calibration, a mean step height on the annealed hematite (0001) surface of 2.2 ± 0.2 Å was obtained by subtracting the average z position of the top terrace from the average z position of the bottom terrace, with the error determined by the root mean square roughness on each terrace. Since the root mean square roughness of each terrace (0.1 Å) matched the noise floor of the AFM, the terraces were interpreted to be atomically flat.

The measured step height of 2.2 ± 0.2 Å agrees well with bulk values of the hematite crystal structure. The distance along the c axis between two adjacent equivalent layers (e.g., oxygen–oxygen or iron–iron layers) in the bulk is 2.29 Å, as indicated in Figure 1a. However, previous reports have suggested that hematite (0001) surfaces can concurrently possess O_3–Fe–Fe–⋯ terminations and Fe–O_3–Fe–⋯ terminations.[21] In this case, differing surface relaxations for the two terminations would lead to deviations in the step height from bulk values.[21,22] For example, Eggleston et al. reported STM data and calculated step heights of 2.3 Å for nonequivalently terminated terraces on the hematite (0001) surface.[23] Using crystal truncation rod diffraction and density functional theory, Trainor et al. have also concluded that mixed domains of O_3–Fe–Fe–⋯ and Fe–O_3–Fe–⋯ terminations exist on the hematite (0001) surface, following surface preparation in oxygen-rich conditions.[24] Consequently, a measured step height of 2.2 ± 0.2 Å is also consistent with adjacent atomically flat domains of nonequivalent surface structure.

Nonequivalent surface domains on hematite (0001) are likely to experience relatively long-range dipolar interactions in

ADVANCED MATERIALS

two dimensions. In this case, Ng and Vanderbilt have shown theoretically that circular (also known as, "droplet") domains are expected to form.[25] Furthermore, this model predicts the possibility of striped domains and even transitions between the striped and droplet domains based upon the details of the surface structure. Previous low-energy electron microscopy (LEEM) data for metal[26] and semiconductor[27] surfaces have confirmed the validity of this theoretical model when non-equivalent surface domains are present. The close similarity of our observed hematite (0001) surface morphologies to these previously reported LEEM data, coupled with the distinct possibility of non-equivalent domains on the hematite (0001) surface, strongly suggests the applicability of the two-dimensional dipolar model to our experimental results.

In conclusion, we have characterized the surface morphology of CVT-grown hematite (0001) at the nanometer scale using AFM. Following annealing under atmospheric pressure in an oxygen-rich environment at 900 °C for 2 h, the surface evolved from a featureless morphology to atomically flat domains that contained 2.2 ± 0.2 Å deep and several hundred nanometer wide circular depressions. The atomically flat domains extend for tens of micrometers and are bound by highly stepped regions. These experimental results are consistent with a two-dimensional dipolar theoretical model for a surface that contains domains of nonequivalent structure. Given the unique electronic and magnetic properties of hematite, the controlled nanoscale surface morphology presented here may be useful for a number of technological applications including catalysis, photoelectrochemistry, magnetic data storage, and spintronics. Furthermore, the long-term air stability of these surfaces suggests that they may serve as effective templates for the growth, patterning, and embossing of nanostructures.

Experimental

Annealing Treatments: As-grown crystals were annealed in a Carbolite single-zone tube furnace (Model STF 15/51/180) equipped with a 99.8 % pure Al_2O_3 tube which was open on both ends. The samples were introduced to the furnace using an unglazed 99.8 % pure Al_2O_3 combustion boat, which was cleaned thoroughly beforehand in aqua regia solution and rinsed in deionized water. The cleaned boat was then dried in a stream of N_2 gas. The samples were heated at 5 °C min^{-1} to 900 °C, held for 2 h, and then cooled at approximately 8 °C min^{-1} to room temperature. During the oxygen or argon flow experiments, the annealing tube was sealed on both ends, and approximately 100 sccm of research-grade O_2 or Ar gas, respectively, flowed through the tube continuously. For the ambient pressure experiments in air, the tube furnace was left unsealed and exposed to the atmosphere.

X-Ray Rocking Curves: As-grown crystal quality was assessed using high-resolution X-ray diffraction (HRXD) at the Northwestern University X-ray Facility. A double crystal spectrometer (Blake Industries) with an angular resolution of 50.0 microradians (μrad) was used to measure the rocking curve for the (0006) Bragg reflection. Cu Kα_1 radiation (1.541 Å) was selected using a dispersive Si (111) 4-bounce monochromator in a + − / − + geometry.

Atomic Force Microscopy: A ThermoMicroscopes CP Research AFM was used to map the topography of the surface before and after annealing. V-shaped Si cantilevers (Ultralevers, ThermoMicroscopes), with a spring constant of 3.2 N m^{-1} and a probe tip with a nominal radius of curvature of 10 nm, were used in intermittent contact mode. Unless otherwise stated, the only image processing performed was a third-order background subtraction to account for nonlinearity in the piezotube scanner.

Received: September 6, 2004
Final version: April 8, 2005

[1] J. W. Geus, *Appl. Catal.* **1986**, *25*, 313.
[2] D. S. Toledano, V. E. Henrich, *J. Phys. Chem. B* **2001**, *105*, 3872.
[3] L. Bandera, K. Tannakone, J. Kiwi, *Langmuir* **2001**, *17*, 3964.
[4] R. M. Cornell, U. Schwertmann, *The Iron Oxides: Structure, Properties, Reactions, Occurrences, and Uses*, Wiley-VCH, Weinheim, Germany **2003**.
[5] J. C. Mallinson, *The Foundations of Magnetic Recording*, Academic Press, San Diego **1987**.
[6] F. J. Morin, *Phys. Rev.* **1954**, *93*, 1195.
[7] W. H. Butler, A. Bandyopadhyay, R. Srinivasa, *J. Appl. Phys.* **2003**, *93*, 7882.
[8] M. A. Chan, B. Beitler, W. T. Parry, J. Ormö, G. Komatsu, *Nature* **2004**, *429*, 731.
[9] T. P. Raming, A. J. A. Winnubst, C. M. van Katz, A. P. Philipse, *J. Colloid Interface Sci.* **2002**, *249*, 346.
[10] S. Lian, E. Wang, Z. Kang, Y. Bai, L. Gao, M. Jiang, C. Hu., L. Xu, *Solid State Commun.* **2004**, *129*, 485.
[11] A. Fujimori, M. Saeki, N. Kimizuka, M. Taniguchi, S. Suga, *Phys. Rev. B* **1986**, *34*, 7318.
[12] R. J. Lad, V. E. Henrich, *Phys. Rev. B* **1989**, *39*, 13 478.
[13] R. L. Blake, R. E. Hessevick, T. Zoltai, L. W. Finger, *Am. Mineral.* **1966**, *51*, 123.
[14] Sh. K. Shaikhutdinov, W. Weiss, *Surf. Sci.* **1999**, *432*, L627.
[15] H. Chang, A. J. Bard, *J. Am. Chem. Soc.* **1990**, *112*, 4598.
[16] P. Heszler, K. Révész, C. T. Reimann, Á. Mechler, Z. Bor, *Nanotechnology* **2000**, *11*, 37.
[17] Á. Mechler, J. Kokavecz, P. Heszler, R. Lal, *Appl. Phys. Lett.* **2003**, *82*, 3740.
[18] G. Koster, G. Rijnders, D. H. A. Blank, H. Rogalla, *Phys. C* **2000**, *339*, 215.
[19] V. P. Kleinert, *Z. Anorg. Allg. Chem.* **1970**, *378*, 71.
[20] K. R. Poeppelmeier, G. B. Ansell, *J. Cryst. Growth* **1981**, *51*, 587.
[21] X.-G. Wang, W. Weiss, Sh. K. Shaikhutdinov, M. Ritter, M. Petersen, F. Wagner, R. Schlögl, M. Scheffler, *Phys. Rev. Lett.* **1998**, *81*, 1038.
[22] O. Warschkow, D. E. Ellis, J. Hwang, N. Mansourian-Hadavi, T. O. Mason, *J. Am. Ceram. Soc.* **2002**, *85*, 213.
[23] C. M. Eggleston, A. G. Stack, K. M. Rosso, S. R. Higgins, A. M. Bice, S. W. Boese, R. D. Pribyl, J. J. Nichols, *Geochim. Cosmochim. Acta* **2003**, *67*, 985.
[24] T. P. Trainor, A. M. Chaka, P. J. Eng, M. Newville, G. A. Waychunas, J. G. Catalano, G. E. Brown, *Surf. Sci.* **2004**, *573*, 204.
[25] K.-O. Ng, D. Vanderbilt, *Phys. Rev. B* **1995**, *52*, 2177.
[26] R. Plass, J. A. Last, N. C. Bartelt, G. L. Kellogg, *Nature* **2001**, *412*, 875.
[27] J. B. Hannon, F.-J. Meyer zu Heringdorf, J. Tersoff, R. M. Tromp, *Phys. Rev. Lett.* **2001**, *86*, 4871.

